Common-path interference and oscillatory Zener tunneling in bilayer graphene p-n junctions

Rahul Nandkishore and Leonid Levitov[1]

Department of Physics, Massachusetts Institute of Technology, Cambridge, MA 02139

Edited by Allan H. MacDonald, The University of Texas, Austin, TX, and approved June 27, 2011 (received for review January 27, 2011)

Interference and tunneling are two signature quantum effects that are often perceived as the yin and yang of quantum mechanics: a particle simultaneously propagating along several distinct classical paths versus a particle penetrating through a classically inaccessible region via a single least-action path. Here we demonstrate that the Dirac quasiparticles in graphene provide a dramatic departure from this paradigm. We show that Zener tunneling in gapped bilayer graphene, which governs transport through p-n heterojunctions, exhibits common-path interference that takes place under the tunnel barrier. Due to a symmetry peculiar to the gapped bilayer graphene bandstructure, interfering tunneling paths form conjugate pairs, giving rise to high-contrast oscillations in transmission as a function of the gate-tunable bandgap and other control parameters of the junction. The common-path interference is solely due to forward-propagating waves; in contrast to Fabry–Pérot-type interference in resonant-tunneling structures, it does not rely on multiple backscattering. The oscillations manifest themselves in the junction I–V characteristic as N-shaped branches with negative differential conductivity. The negative dI/dV, which arises solely due to under-barrier interference, can enable new high-speed active-circuit devices with architectures that are not available in electronic semiconductor devices.

graphene heterojunctions | nanodevices | quantum transport | quartic dispersion | quasiclassical approximation

Quantum tunneling through two or more barriers that are placed closely together is characterized by transmission that is sharply peaked about certain energies. Such "resonant-tunneling" effect arises because particles can reflect between the barriers and resonate at particular energies, allowing enhanced transmission through the barriers. This resonance phenomenon is similar to that taking place in optical Fabry–Pérot resonators. Resonant tunneling is particularly desirable in applications because it can give rise to negative differential resistance—current that goes down as voltage goes up—an interesting behavior that can be harnessed to form new devices (1, 2).

Here we propose an entirely different approach to realize oscillatory transmission, which involves only *forward-propagating* waves and a *single* barrier, and thus is distinct from the Fabry–Pérot interference of waves undergoing multiple reflection between two barriers. This behavior arises in graphene bilayer (3, 4), a two-dimensional semiconductor material with unique electronic properties, such as the field effect and the possibility to open a bandgap by using external gates (5, 6, 7). We demonstrate that Zener tunneling in a p-n junction in gapped bilayer graphene (BLG) exhibits common-path interference taking place under the tunnel barrier, leading to transmission that oscillates as a function of gate-tunable bandgap. This unique behavior enables device architectures that are not possible in other gapped materials.

Unlike the conventional tunneling through a potential barrier, Zener tunneling is governed by an externally applied electric field (8). Strong enough fields, by mixing states in different bands, can induce transitions from the valence band of a p-type material to the conduction band of an n-type material, giving rise to tunneling currents. In conventional semiconductors, the tunneling rate is a monotonic function of the applied field F and the bandgap E_g, given by an exponential $\exp(-\pi m^{1/2}E_g^{3/2}/2F\hbar)$ (here m is an effective mass) (9, 10). In a sharp departure from this behavior, we find that transmission through a p-n junction in BLG *oscillates* as a function of the bandgap and external field. At normal incidence, the oscillations have 100% contrast, with transmission vanishing at particular nodal values of control parameters (see Fig. 1). The oscillations remain high-contrast after the transmission is averaged over incidence angles. The common-path nature of the interference renders this phenomenon insensitive to Aharanov–Bohm type dephasing effects.

Relativistic-like behavior of carriers in graphene leads to many interesting transport phenomena (11–15). However, the effects discussed here have not been anticipated. Conventional Zener tunneling was studied in p-n junctions in semiconducting carbon nanotubes (16, 17) and single-layer graphene (18). Theory of these systems (19, 20) yields exponential dependences that match closely those of refs. 9 and 10. Similar exponential dependence arises in the theory of p-n junctions in gated gapless graphene sheets (21), with a momentum component along the p-n interface playing the role of a bandgap.

The origin of the oscillatory behavior can be elucidated by a semiclassical analysis of the dynamics in the barrier region. In contrast to the standard case of tunneling through a one-dimensional barrier, where a unique saddle-point trajectory in a classically forbidden region is found for each energy, here we obtain multiple trajectories. Further, the trajectories form pairs with *complex conjugate* Wentzel–Kramers–Brillouin (WKB) action values S and S^*. Common-path interference of such pairs gives rise to an oscillatory transmission

$$T = \left|ae^{-\frac{1}{\hbar}S} + a^*e^{-\frac{1}{\hbar}S^*}\right|^2 = 4|a|^2e^{-\frac{2}{\hbar}S'}\cos^2\left(\frac{S''}{\hbar}+\varphi\right), \qquad [1]$$

where $S = S' + iS''$. Both S' and S'' are monotonic functions of the bandgap and field strength (see Eq. **4**). The oscillations in transmission will manifest themselves through negative differential conductivity in the I–V characteristic.

This unique behavior opens a door for designing new device architectures. Small intrinsic capacitance of planar heterojunctions can enable high-speed devices. Further, the single-particle effects responsible for the negative dI/dV are completely insensitive to the behavior in the doped regions, which is a distinct advantage compared to many resonant-tunneling devices (1) whose performance is limited by their relatively high capacitance and by thermal stability of dopants.

Author contributions: R.N. and L.L. performed research; L.L. designed research; and R.N. and L.L. wrote the paper.

The authors declare no conflict of interest.

This article is a PNAS Direct Submission.

[1]To whom correspondence should be addressed. E-mail: levitov@mit.edu.

This article contains supporting information online at www.pnas.org/lookup/suppl/doi:10.1073/pnas.1101352108/-/DCSupplemental.

Model: The WKB Analysis

To clarify the origin of Eq. **1**, we first consider transmission using the WKB formalism. Gapped BLG in the presence of a barrier potential $V(x)$ is described by a 2×2 quadratic Dirac Hamiltonian (4)

$$H=\begin{pmatrix}\Delta & \frac{1}{2m}(p_x+ip_y)^2\\ \frac{1}{2m}(p_x-ip_y)^2 & -\Delta\end{pmatrix}+V(x),\qquad \Delta=\frac{E_g}{2}, \quad [2]$$

where E_g is the bandgap. We seek the wavefunction in the barrier region in the form

$$\psi(x)\propto e^{\frac{i}{\hbar}\int_{x_0}^{x}p(x')dx'}\chi,$$

where χ is a two-component spinor. The x dependence of momentum can be found from the energy integral $E=\pm[(p^2/2m)^2+\Delta^2]^{1/2}+V(x)$. In the barrier region, $-\Delta<V(x)-E<\Delta$, this relation gives four complex roots

$$p_x(x)=\pm\sqrt{-p_y^2\pm 2mi\sqrt{\Delta^2-(V(x)-E)^2}}, \quad [3]$$

where p_y is a conserved y component of momentum. Two of the roots (**3**) have $\mathrm{Im}p>0$, and the other two have $\mathrm{Im}p<0$. Positive (negative) Imp correspond to decaying (growing) exponentials which describe particle propagation to the right and to the left, respectively.

Focusing on the uniform-field model $V(x)=-Fx$ (see Fig. 1, *Inset*) and for simplicity setting $p_y=0$, we select from (**3**) the right-propagating solutions: $p_\pm(x)=(i\pm 1)m^{1/2}[\Delta^2-(Fx-E)^2]^{1/4}$. These two solutions give complex conjugate WKB transition amplitudes $e^{-S/\hbar}$, $e^{-S^*/\hbar}$, where

$$S,S^*=(1\pm i)\alpha m^{1/2}\Delta^{3/2}/F \quad [4]$$

with the prefactor expressed through the Euler beta function, $\alpha=\mathrm{B}(\frac{1}{2},\frac{5}{4})\approx 1.75$.

The total transmission amplitude in the WKB approximation is the sum of the transmission amplitudes for the two decaying exponentials. Combining the contributions of the trajectories $p_\pm(x)$, we can write the WKB wavefunction in the barrier region as a sum

$$ae^{\frac{i}{\hbar}\int_{x_0}^{x}p_+(x')dx'}+a^*e^{\frac{i}{\hbar}\int_{x_0}^{x}p_-(x')dx'}.$$

Interference between these evanescent solutions produces an oscillatory transmission amplitude

$$A=ae^{-S/\hbar}+a^*e^{-S^*/\hbar}. \quad [5]$$

Because $\mathrm{Re}S=\mathrm{Re}S^*$ and $\mathrm{Im}S=-\mathrm{Im}S^*$, the two contributions to the transmission amplitude are of equal magnitude and differ in phase by $\Delta\theta=2(\frac{1}{\hbar}\mathrm{Im}S-\varphi)$. Here, $\varphi=\arg(a)$ is a phase offset between the two decaying exponentials, which can in principle be obtained by matching solutions at the classical turning points, but in practice is more easily obtained through a numerical procedure, which gives $\varphi\approx\pi/2$ (see Fig. 2 and accompanying discussion).

For certain nodal values of F and Δ, the interference is destructive and the transmission probability vanishes. Plugging the values (**4**) in Eq. **5**, we see that the transmission probability $T=|A|^2$ oscillates, going through nodes when $\alpha m^{1/2}\Delta^{3/2}/F\hbar$ is an integer multiple of π. This condition gives the nodal values

$$\Delta_n=(\pi n/\alpha)^{2/3}(F^2\hbar^2/m)^{1/3},\qquad n=1,2,3,... \quad [6]$$

that match closely the nodes found numerically (Fig. 1). The dip in transmission at $E_g=0$ originates from the chirality-assisted suppression of tunneling in gapless BLG (see ref. 22).

The oscillations in transmission, being a general feature deriving from interference, are a robust and generic phenomenon. In particular, the oscillations do not require a linear potential in the barrier region, and the WKB analysis may be straightforwardly generalized to an arbitrary potential profile $V(x)$. Weak perturbations to the BLG dispersion also can be easily incorporated in the above analysis and shown not to matter as long as the perturbation strength is weak compared to the gap Δ. For example, the trigonal warping interaction can affect the dispersion within a few millielectronvolts of the Dirac point (4), thus its effect will be small in systems with gate-induced gap that can reach a few hundred millielectronvolts (7).

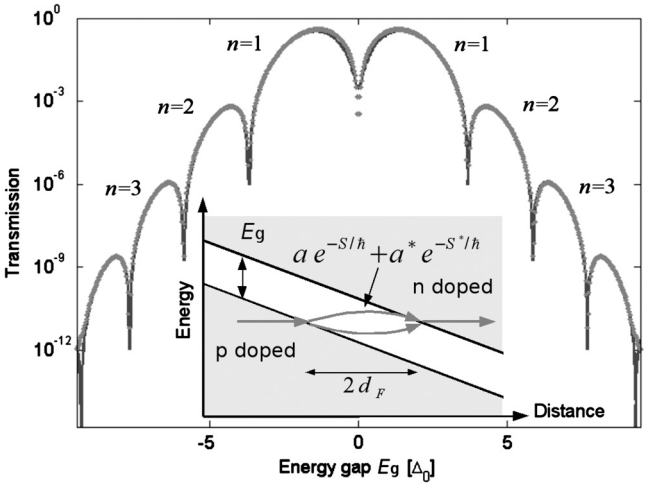

Fig. 1. Zener tunneling and common-path interference in BLG in the uniform-field model. Interference of two least-action tunneling paths results in oscillations, $n=1,2,...$. Shown is transmission at normal incidence, $p_y=0$, as a function of bandgap size, in units $\Delta_0=[(F\hbar)^2/2m]^{1/3}$ (semilog scale). Numerical results (red symbols), obtained by integrating Eq. **8**, agree with the WKB result, Eqs. **1** and **4** (blue curve) in the entire range of Δ, large and small. Inset shows schematic setup of p-n junction: The bandgap $E_g=2\Delta$, the linear barrier potential $V(x)=-Fx$ (see Eq. **2**), and a pair of interfering tunneling paths.

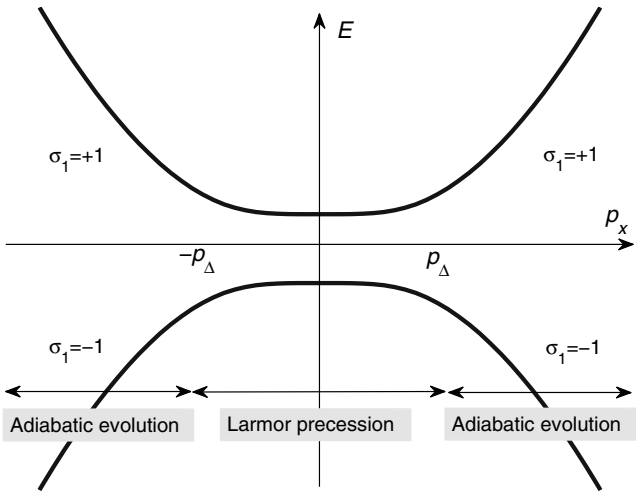

Fig. 2. Evolution of a two-level system slowly driven through an avoided level crossing, Eq. **8**. Nonadiabatic transitions between different levels, corresponding to Zener tunneling, take place in the Larmor precession region $-p_\Delta\lesssim p\lesssim p_\Delta$, where $p_\Delta=\sqrt{2m\Delta}$. Shown are adiabatic energy levels of the Hamiltonian, Eq. **8** (blue line) and schematic partition into regions of adiabatic evolution and Larmor precession.

Another requirement on experimental systems in which the interference phenomena described above can be realized is that of ballistic transport in the p-n junction region. Recent observation of Fabry–Pérot (FP) oscillations in graphene p-n-p junctions (24) provides a clear signature of ballistic transport in this system. The oscillation could be seen for the p-n interface separation of up to 60 nm, which sets a lower bound on the mean free path in the presence of a top gate. For a rough estimate, writing $F = U/L$ with U a gate-induced potential difference across a p-n junction and L the junction width (see Fig. 3, *Inset*), from Eq. **6** we predict the number of experimentally accessible nodes

$$n \approx \frac{\alpha}{\pi}\frac{m^{1/2}\Delta^{3/2}}{F\hbar} = \frac{\alpha}{\pi\sqrt{2}}\frac{\Delta}{eU}\frac{L}{\ell_\Delta}, \qquad \ell_\Delta = \frac{\hbar}{\sqrt{2m\Delta}}. \qquad [7]$$

For $\Delta = 100$ meV, and using the effective mass in BLG $m = 0.033\, m_0$, we estimate the characteristic lengthscale $\ell_\Delta \approx$ 3.18 nm. Taking $eU = 4\Delta$ and $L = 60$ nm, we arrive at $n \approx 4$, which indicates that oscillatory Zener tunneling is well within reach of current experiments.

Discussion: Zener Tunneling in Momentum Space.
We now explain the origin of the oscillations from a different perspective, by mapping the transmission across the p-n junction to evolution of a two-level system which is swept through an avoided level crossing. This alternative formalism is specialized for the uniform-field model, and thus is less general than the WKB method. However, it provides intuition and affords an independent check on the WKB results by allowing us to numerically evaluate the transmission probability without any undetermined phase offsets.

The key to this alternative formulation is an observation that, for the uniform-field model $V(x) = -Fx$, the problem greatly simplifies in the momentum representation. Indeed, because $x = i\hbar\partial_{p_x}$, the Schrodinger equation with the Hamiltonian **[2]** turns into a first-order differential equation

$$i\hbar F\frac{\partial\psi}{\partial p_x} = \left(\frac{p_x^2 - p_y^2}{2m}\sigma_1 + \frac{2p_xp_y}{2m}\sigma_2 + \Delta\sigma_3\right)\psi, \qquad [8]$$

where the σ_i are the Pauli matrices in sublattice space. This equation is identical to the time-dependent Schrodinger equation for a spin-half wavefunction with p_x playing the role of time.

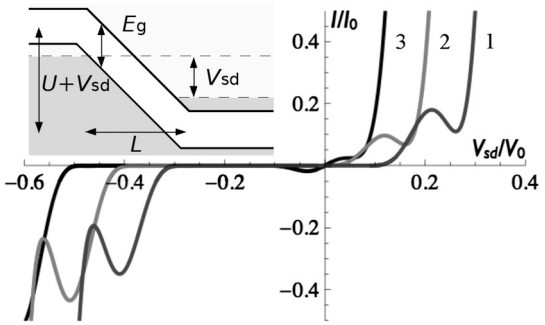

Fig. 3. The *I–V* characteristic of a BLG p-n junction combines features of Esaki diode (N-shaped branches with negative differential conductivity) and Zener diode (a breakdown-type behavior). Thus a single p-n junction can serve as an active-circuit element with multiple functionality. Valleys in the *I–V* dependence correspond to $n = 1$ node of the oscillations in transmission in Fig. 1. Shown is the *I–V* dependence given by Eq. **11** for parameter values: $U/V_0 = 0.1, 0.2, 0.3$ (curves 1, 2, and 3, respectively). Units are $V_0 = \Delta(L/\ell_\Delta)$ and $I_0 = 10^{-4}N\frac{e^2}{h}(W/2\pi\ell_\Delta)V_0$, where W is the lateral width of the junction and $N = 4$ is the spin/valley degeneracy in BLG. Inset shows junction schematic, with U the built-in potential induced by doping or by gates, and $E_g = 2\Delta$ the bandgap.

There is a simple relation between the "time evolution" governed by Eq. **8** and interband transitions induced by Zener tunneling (25). Asymptotically, at $p_x \to \pm\infty$, the eigenstates of the Hamiltonian are also eigenstates of σ_1, having energies $E_{\sigma_1=\pm1} = \mp p_x^2/2m$. As we tune p_x from $-\infty$ to $+\infty$, the system is swept through an avoided level crossing, as illustrated in Fig. 2. Interband transitions are described by the process in which a state that started off in the $\sigma_1 = -1$ eigenstate at $p_x = -\infty$ will evolve into the $\sigma_1 = +1$ eigenstate at $p_x = +\infty$. The evolution is near-adiabatic at small F, with Zener tunneling described as (nonadiabatic) transitions across the gap.

In this framework, the oscillations in transmission can be understood in a simple and intuitive way by noting that the Heisenberg evolution of momentum $p_x(t)$ corresponds to sweeping through the avoided crossing at a constant speed, $dp_x/dt = F$. Comparing different terms in Eq. **8**, we conclude that transitions may only happen in the region $-p_\Delta \lesssim p_x \lesssim p_\Delta$, where $p_\Delta = \sqrt{2m\Delta}$ (see Fig. 2), whereas outside this region the evolution is adiabatic (here we set $p_y = 0$ for simplicity). In the transition region, the dominant term in the Hamiltonian is $\Delta\sigma_3$. Spin rotation caused by this term can be described as Larmor precession about the z axis by an angle $\delta\theta = (\Delta/\hbar F)p_\Delta$. Periodic modulation of the transition rate of the form $\cos\delta\theta$, resulting from Larmor precession, leads to an estimate of the oscillation period that agrees with the WKB result, Eqs. **1** and **4**.

The momentum-sweep analysis also helps to understand the dramatic difference between transmission in bilayer junctions and single-layer junctions. The latter problem can be mapped (26) to a canonical Landau Zener problem of a linear sweep through an avoided level crossing, for which transmission is a monotonic function of control parameters exhibiting no oscillations. This result is in agreement with the theory of p-n junctions in single-layer graphene (21).

In light of this analogy, it is interesting to compare our Larmor-type oscillations with the Stückelberg oscillations arising in systems that are swept multiple times through a level crossing (27). Because our oscillations occur in a single sweep, they are more robust to dephasing and decoherence. Whereas Stückelberg oscillations occur when the system remains phase coherent between consecutive sweeps, here only phase coherence over the timescale of a single sweep is necessary.

Results: The *I–V* Characteristic.
We now place this discussion on a firm quantitative ground by calculating the transition probability numerically. We solve the differential equation, Eq. **8**, in a suitably chosen interval $p_{\min} < p_x < p_{\max}$, taking as the initial state at $p_x = p_{\min}$ the adiabatic ground state. From the numerical solution, we determine the probability to evolve into the excited state at $p_x = p_{\max}$. The transmission probability, obtained in this manner for $p_y = 0$ and $p_{\max(\min)} = \pm 22p_\Delta$, is shown in Fig. 1. The results are compared with the prediction of the WKB approach, Eq. **1**, treating the prefactor $|a|^2$ and the phase φ as fitting parameters. As illustrated in Fig. 1, excellent agreement is found for the values $\varphi = 1.6$ and $|a|^2 = 0.78$ (which are tantalizingly close to $\pi/2$ and $\pi/4$), indicating that the WKB analysis provides reliable results.

Integrating Eq. **8** at finite p_y, we find that the transmission oscillates and vanishes at nodal values of Δ in pretty much the same way as for zero p_y. Comparing to the WKB analysis, which continues to apply at finite p_y, we find that the WKB phase offset $\varphi(p_y)$ varies only weakly with p_y. Using this numerical procedure, we may also straightforwardly take into account trigonal warping. Apart from a weak washing out of the nodes, we find no significant effect on the oscillations of transmission provided the trigonal warping energy scale is less than the gap size.

Next, we proceed to show that the oscillatory tunneling reveals itself through distinct features in the *I–V* characteristic. The net tunneling current can be expressed, according to the Landauer

formula (14), as a sum of contributions of all conducting channels multiplied by energy distribution in reservoirs, giving

$$I = \frac{e}{h}\int_{-\infty}^{\infty} dE(n_{E-\frac{1}{2}eV_{\rm sd}} - n_{E+\frac{1}{2}eV_{\rm sd}})\mathbf{T}(F), \qquad [9]$$

$$\mathbf{T}(F) = \frac{NW}{2\pi\hbar}\int_{-\infty}^{\infty} dp_y T_{p_y,E}(F), \qquad [10]$$

where W is the total length of the p-n interface, and the factor $N = 4$ is spin/valley degeneracy in BLG. Here, accounting for the fact that transmission is dominated by small values of p_y (see below), we treat the occupation numbers as p_y independent and factor out the quantity $\mathbf{T}(F)$, the net transmission integrated over p_y.

Continuing to work with the uniform-field model, we treat transmission as energy independent and incorporate the source-drain voltage in the effective barrier potential via $F = F_0 + eV_{\rm sd}/L$ (see Fig. 3, *Inset*). Integrating over energies, we have

$$I = \frac{e^2}{h}V_{\rm sd}\mathbf{T}(F_0 + eV_{\rm sd}/L), \quad F_0 = eU/L. \qquad [11]$$

The dependence of transmission T_{p_y} on p_y may be found from Eq. **1** with $S(p_y)$ and $S^*(p_y)$ evaluated using Eq. **3**. Because the transmission is exponentially small in the barrier width, and the width of the barrier region grows monotonically with p_y^2, the net transmission $\mathbf{T}$ is dominated by small values of p_y. Hence, we may approximate S and S^* as

$$S,S^* = i^{\pm 1/2}\alpha\frac{\Delta p_\Delta}{F} + i^{\mp 1/2}\frac{\tilde{\alpha}\Delta}{2Fp_\Delta}p_y^2 + O(p_y^4), \qquad [12]$$

where $\tilde{\alpha} = \sqrt{2}B(\frac{3}{4},\frac{3}{4}) \approx 2.4$. Plugging these expressions in Eq. **1** and performing Gaussian integration over p_y, we find

$$\mathbf{T}(F) = \frac{NW|a|^2F^{1/2}}{(\pi\tilde{\alpha}\Delta\ell_\Delta)^{1/2}}e^{-\frac{2}{\hbar}S'}\left[2^{1/4} + \cos\left(\frac{2}{\hbar}S'' + \tilde{\varphi}\right)\right], \qquad [13]$$

$\tilde{\varphi} = 2\varphi - \frac{\pi}{8}$, where S' and S'' are given by Eq. **4**. Based on numerical results, we ignored the p_y dependence of the phase offset φ in Eq. **1**. Interestingly, the resulting I–V curve, Eq. **11**, exhibits *negative differential conductivity*.

A more accurate result for the net transmission $\mathbf{T}$ can be obtained by numerical integration of the exact WKB transmission over momenta (*SI Appendix*). In that, the full dependence of S and S^* on p_y is retained, and also the contribution of the classically forbidden regions $\Delta < |Fx - E| < \sqrt{\Delta^2 + (p_y^2/2m)^2}$ is included, which is of subleading order in p_y^2.

The resulting I–V dependence is shown in Fig. 3 for several values of the "built-in" (gate-induced) potential difference across the p-n junction. Notably, the I–V characteristic combines features of the Zener diode (sharp rise of current above certain breakdown voltage) with N-shaped branches on which the differential conductivity is negative, resembling the resonant-tunneling (Esaki) I–V characteristic (23). Unlike the Esaki characteristic, the N-shaped branches occur simultaneously on the forward and reverse parts of the I–V dependence. The N-shaped features arise from oscillations in single-particle transmission, a mechanism very different from that leading to negative dI/dV in the Esaki diode. The valleys of current in Fig. 3 correspond to nodes of transmission ($n = 1$ in Fig. 1).

Conclusions

The p-n junctions of the type considered here can be realized using a configuration of gates which is already employed in current experiments (6, 24, 28, 29). A minimal configuration is a dual-gate geometry with a wide back gate and a narrow top gate, such as that used in the work on FP oscillations (24). Charging the two gates with voltages of opposite polarity, a bandgap can be induced under the top gate and, simultaneously, carrier density can be adjusted in the outer region. Applying source-drain bias will produce $V_{\rm sd}$-dominated lateral electric field across the gapped region, corresponding to the regime $U \ll V_0$ where the effect of oscillations is most prominent (see Fig. 3). In addition, a built-in field U can be induced by selective doping or by a third gate.

In summary, transport in BLG p-n junctions is governed by common-path interference under the tunnel barrier. Unlike Fabry–Pérot interference that stems from multiple reflection between barriers, our interference effect involves only forward-propagating paths and a single barrier. The interference produces nodes in transmission as a function of the gate-tunable bandgap and other control parameters, leading to an I–V characteristic that features N-shaped branches with negative differential conductivity. Low capacitance of lateral heterojunctions can enable high-speed operation. The single-particle origin of negative dI/dV makes it insensitive to the behavior in the doped regions, unlike many resonant-tunneling devices where performance is limited by thermal stability of the dopants (1). We envision that BLG p-n junctions, owing to their multiple functionality and design simplicity, will become an integral part of the future graphene electronics toolkit.

1. Sze SM, Ng KK (2007) *Physics of Semiconductor Devices* (Wiley, New York).
2. Esaki L, Tsu R (1970) Superlattice and negative differential conductivity in semiconductors. *IBM J Res Dev* 14:61–65.
3. Novoselov KS, et al. (2006) Unconventional quantum Hall effect and Berry's phase of 2π in bilayer graphene. *Nat Phys* 2:177–180.
4. McCann Em, Fal'ko VI (2006) Landau-level degeneracy and quantum hall effect in a graphite bilayer. *Phys Rev Lett* 96:086805.
5. McCann E (2006) Asymmetry gap in the electronic band structure of bilayer graphene. *Phys Rev B* 74:161403(R).
6. Oostinga JB, Heersche HB, Liu X, Morpurgo AF, Vandersypen LMK (2007) Gate-induced insulating state in bilayer graphene devices. *Nat Mater* 7:151–157.
7. Zhang Y, et al. (2009) Direct observation of a widely tunable bandgap in bilayer graphene. *Nature* 459:820–823.
8. Zener CA (1934) Theory of the electrical breakdown of solid dielectrics. *Proc R Soc London* 145:523–529.
9. Keldysh LV (1957) Behavior of non-metallic crystals in strong electric fields. *J Exp Theor Phys (USSR)* 33:994–1003.
10. Kane EO (1959) Zener tunneling in semiconductors. *J Phys Chem Solids* 12:181–188.
11. Katsnelson MI, Novoselov KS, Geim AK (2006) Chiral tunnelling and the Klein paradox in graphene. *Nat Phys* 2:620–625.
12. Cheianov VV, Falko V, Altshuler BL (2007) The focusing of electron flow and a Veselago lens in graphene p-n junctions. *Science* 315:1252–1255.
13. Martin I, Blanter YM, Morpurgo AF (2008) Topological confinement in bilayer graphene. *Phys Rev Lett* 100:036804.
14. Beenakker CWJ (2008) Colloquium: Andreev reflection and Klein tunneling in graphene. *Rev Mod Phys* 80:1337–1354.
15. Castro Neto AH, Guinea F, Peres NMR, Novoselov KS, Geim AK (2009) The electronic properties of graphene. *Rev Mod Phys* 81:109–162.
16. Appenzeller J, Lin YM, Knoch J, Avouris P (2004) Band-to-band tunneling in carbon nanotube field-effect transistors. *Phys Rev Lett* 93:196805.
17. Bosnick K, Gabor N, McEuen PL (2006) Transport in carbon nanotube p-i-n diodes. *Appl Phys Lett* 89:163121.
18. Vandecasteele N, Barreiro V, Lazzeri M, Bachtold A, Mauri F (2010) Current-voltage characteristics of graphene devices: Interplay between Zener-Klein tunneling and defects. *Phys Rev B* 82:045416.
19. Andreev AV (2007) Magnetoconductance of carbon nanotube p-n junctions. *Phys Rev Lett* 99:247204.
20. Jena D, Fang T, Zhang Q, Xing H (2008) Zener tunneling in semiconducting nanotube and graphene nanoribbon pn junctions. *Appl Phys Lett* 93:112106.
21. Cheianov VV, Falko VI (2006) Selective transmission of Dirac electrons and ballistic magnetoresistance of n-p junctions in graphene. *Phys Rev B* 74:41403(R).
22. Gu N, Rudner MS, Levitov LS (2011) Chirality-Assisted Electronic Cloaking in Bilayer Graphene Nanostructures. *Phys Rev Lett* arXiv:1106.1142.
23. Esaki L (1958) New phenomenon in narrow germanium p-n junctions. *Phys Rev* 109:603–604.

24. Young AF, Kim P (2009) Quantum interference and Klein tunneling in graphene heterojunctions. *Nat Phys* 5:222–226.
25. Kane EO, Blount E (1969) *Tunneling Phenomena in Solids*, eds E Burnstein and S Lundqvist (Plenum, New York), pp 79–91.
26. Shytov A, Gu N, Levitov L (2007) Transport in graphene p-n junctions in magnetic field. arXiv:0708.3081v1.
27. Stückelberg ECG (1932) Theory of inelastic collisions between atoms. *Helv Phys Acta* 5:369–422.
28. Huard B, et al. (2007) Transport measurements across a tunable potential barrier in graphene. *Phys Rev Lett* 98:236803.
29. Williams JR, DiCarlo L, Marcus CM (2007) Quantum Hall effect in a gate-controlled p-n junction of graphene. *Science* 317:638–641.